Lawrence Berkeley National Laboratory

LBL Publications

Title

Facile bottom-up synthesis of partially oxidized black phosphorus nanosheets as metal-free photocatalyst for hydrogen evolution

Permalink

https://escholarship.org/uc/item/2w68b0n2

Journal

Proceedings of the National Academy of Sciences of the United States of America, 115(17)

ISSN

0027-8424

Authors

Tian, Bin

Tian, Bining

Smith, Bethany

et al.

Publication Date

2018-04-24

DOI

10.1073/pnas.1800069115

Peer reviewed

eScholarship.org Powered by the California Digital Library
University of California

SEE COMMENTARY

Facile bottom-up synthesis of partially oxidized black phosphorus nanosheets as metal-free photocatalyst for hydrogen evolution

Bin Tian[a,1], Bining Tian[a,1], Bethany Smith[b,c], M. C. Scott[b,c], Qin Lei[a], Ruinian Hua[d], Yue Tian[a,c,2], and Yi Liu[c,2]

[a]Key Laboratory of Advanced Transducers and Intelligent Control System of Ministry of Education, College of Physics and Optoelectronics, Taiyuan University of Technology, 030024 Taiyuan, China; [b]Department of Materials Science and Engineering, University of California, Berkeley, CA 94720; [c]Molecular Foundry, Lawrence Berkeley National Laboratory, Berkeley, CA 94720; and [d]College of Life Science, Dalian Nationalities University, Liaoning, 116600 Dalian, China

Edited by Christopher Cummins, Massachusetts Institute of Technology, Cambridge, MA, and approved February 27, 2018 (received for review January 3, 2018)

Few-layer black phosphorus (BP) nanosheets were first reported as a 2D material for the application of field-effect transistors in 2014 and have stimulated intense activity among physicists, chemists, and material and biomedical scientists, driving research into novel synthetic techniques to produce BP nanosheets. At present, exfoliation is the main route toward few-layer BP nanosheets via employing bulk BP as raw material. However, this is a complicated and time-consuming process, which is difficult for the large-scale synthesis of BP nanosheets. Moreover, BP degrades rapidly when exfoliated to nanoscale dimensions, resulting in the rapid loss of semiconducting properties. Here, we report the direct wet-chemical synthesis of few-layer BP nanosheets in gram-scale quantities in a bottom-up approach based on common laboratory reagents at low temperature, showing excellent stability due to partial oxidation of surface. Solvent and temperature are two critical factors, controlling not only the formation of BP nanosheets but also the thickness. The as-prepared BP nanosheets can extract hydrogen from pure water (pH = 6.8), exhibiting more than 24-fold higher activity than the well-known C_3N_4 nanosheets. Our results reporting the ability to prepare few-layer BP nanosheets with a facile, scalable, low-cost approach take us a step closer to real-world applications of phosphorene including next-generation metal-free photocatalysts for photosynthesis.

black phosphorus | 2D materials | bottom-up synthesis | photocatalysis | hydrogen evolution

Besides the most commonly seen white and red phosphorus, black phosphorus (BP) is another allotrope of phosphorus exhibiting semiconductor-like properties with a thickness-dependent band gap, which has been emerging as a promising 2D material for applications in photoelectronic devices, biomedicine, catalysis, and energy storage since the recognition of its anisotropic 2D layered structure (1–11). BP was found to have cubic, orthorhombic, rhombohedral, and amorphous phase structures (5). Orthorhombic BP nanosheets, consisting of puckered layers stacked together by strong intralayer bonding and weak interlayer van der Waals interactions, offer fascinating advantages over graphene and transition-metal dichalcogenides because of its unique in-plane anisotropy and high charge-carrier mobility (1, 12). To achieve success in the wide applications, easy access to BP nanosheets is crucial. The earliest report on the synthesis of BP can be traced back to a century ago (13), where bulk BP was obtained via employing white phosphorus as raw material at a high pressure of 1.2 GPa and 200 °C. Despite tremendous efforts devoted to the synthesis (14–16), it is still not easy to synthesize bulk BP. Moreover, all of the known methods focused on the synthesis of bulk BP, but not on its nanosheet form, which is of interest here. The first few-layer BP nanosheets were produced via mechanical exfoliation of bulk BP until 2014 (1). At present, exfoliation including mechanical and solution-based exfoliation has been the most common route toward few-layer BP nanosheets. However, this two-step synthesis process for the production of BP nanosheets, in which high-quality bulk BP needs to be prepared first, renders the synthesis of BP nanosheets complicated, time-consuming, and costly. Moreover, the scalable synthesis of BP nanosheets with excellent stability is still a challenge via exfoliation technique, restricting the wide study and applications of BP nanosheets.

Results and Discussion

Given the lack of a low-cost solution-based approach for the large-scale production of BP nanosheets, here we report the one-pot wet-chemical synthesis of BP nanosheets in gram-scale quantities using white phosphorus as raw materials and ethylenediamine as solvent, operated at low temperature (Fig. 1*A*). X-ray diffraction (XRD) taken from the as-prepared powder samples confirms orthorhombic (Cmca) crystal structure of BP without any other phases (Fig. 1*B*). Moreover, the XRD intensity increases with the increase of temperature, indicating improved crystallinity (*SI Appendix*, Fig. S1). Energy-dispersive X-ray spectral analysis (EDX) shows that the product mainly consists of phosphorus element (*SI Appendix*, Fig. S2). These results

Significance

Black phosphorus (BP) nanosheet is a "hot" class of 2D material having wide applications in optoelectronics, catalysis, biomedicine, etc. However, facile synthesis of BP nanosheets is not achieved by far. Currently, BP nanosheets are mainly prepared via solution-based exfoliation of bulk crystals, a process that is complicated, time-consuming, and costly. Moreover, the as-prepared BP nanosheets are not stable. Here, we developed a facile bottom-up protocol for preparing BP nanosheets in solution at low temperature. Our synthetic procedure is conceptually simple and can be performed in common chemical laboratories. The estimated synthesis cost is less than 1 US dollar per gram. Our work, therefore, offers the community an unlimited access to such 2D material.

Author contributions: Y.T. and Y.L. designed research; Bin Tian and Bining Tian performed research; B.S. and M.C.S. contributed new reagents/analytic tools; Bin Tian, Bining Tian, Q.L., R.H., Y.T., and Y.L. analyzed data; and Bin Tian, Bining Tian, M.C.S., Y.T., and Y.L. wrote the paper.

The authors declare no conflict of interest.

This article is a PNAS Direct Submission.

This open access article is distributed under Creative Commons Attribution-NonCommercial-NoDerivatives License 4.0 (CC BY-NC-ND).

See Commentary on page 4311.

[1]Bin Tian and Bining Tian contributed equally to this work.

[2]To whom correspondence may be addressed. Email: tianyue@tyut.edu.cn or yliu@lbl.gov.

This article contains supporting information online at www.pnas.org/lookup/suppl/doi:10.1073/pnas.1800069115/-/DCSupplemental.

Published online March 21, 2018.

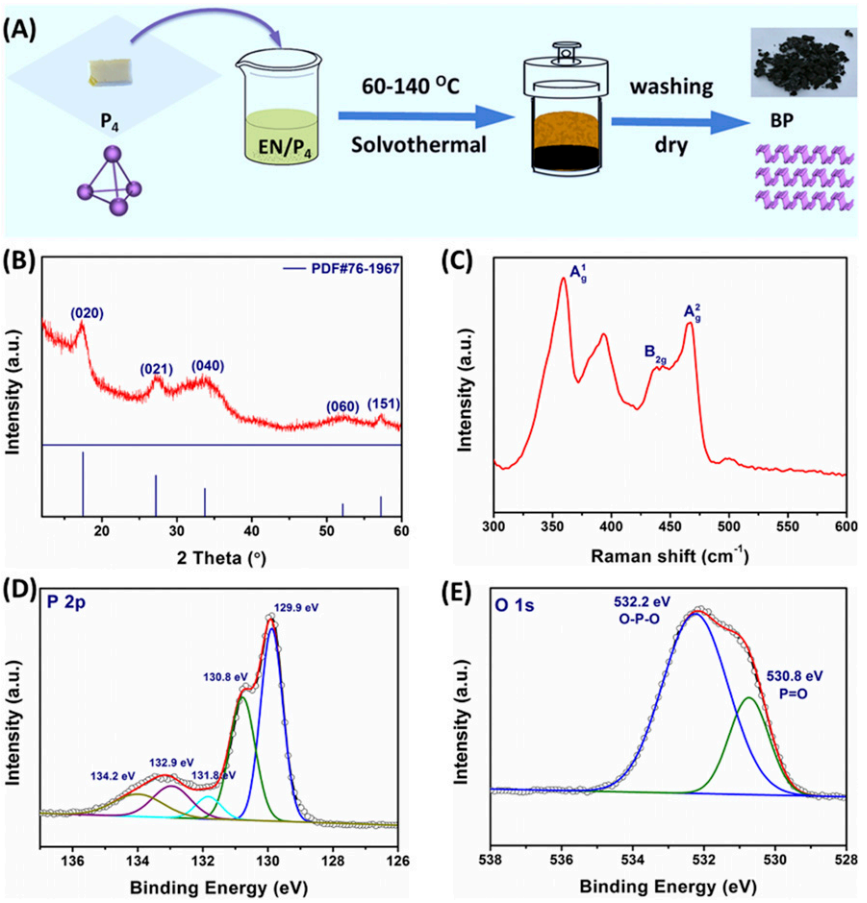

Fig. 1. Synthetic protocol and spectroscopic analysis of the BP. (*A*) Few-layers BP nanosheets were synthesized through a solvothermal process at the temperature range of 60–140 °C using white phosphorus as raw material and ethylenediamine (EN) as solvent. The image shows ~2 g of sample. (*B*) XRD pattern of the BP nanosheets obtained at 100 °C. Peaks are labeled based on the orthorhombic lattice of BP. (*C*) Raman spectrum. The excitation wavelength is 633 nm. (*D* and *E*) XPS fine spectra of P 2p and O 1s in the BP nanosheets. The C 1s (284.8 eV) is the charged correction benchmark.

suggest that BP can be prepared directly via a facile solvothermal process at low temperature. The typical Raman peaks located at 360.2, 437.5, and 464.6 cm^{-1} (Fig. 1*C*) can be observed in the BP sample obtained at 100 °C, corresponding to the characteristic A^1_g, B_{2g}, and A^2_g modes of BP (17). These results further confirm the formation of BP. Besides these three peaks, another peak at about 400 cm^{-1} could be assigned to the P-O species because of partial oxidation (18). Furthermore, the BP samples prepared at the temperature range of 60–140 °C exhibit quite similar Raman spectral profiles (*SI Appendix*, Fig. S3), further confirming that BP can be obtained at this temperature range.

The as-prepared BP samples were also analyzed using X-ray photoemission spectroscopy (XPS). All of the XPS spectra exhibit a very similar feature with two narrow peaks in the range of 128–131 eV along with a broad band ranging from 131 to 136 eV (Fig. 1*D* and *SI Appendix*, Fig. S4). The two peaks at 129.9 and 130.8 eV correspond to the $2p_{3/2}$ and $2p_{1/2}$ states of P element (2). The broad band can be deconvoluted into three peaks at 131.8, 132.9, and 134.2 eV, attributed to P-O-P, O-*P* = O, and P_2O_5 (19), respectively. O1s XPS spectrum (Fig. 1*E*) further reveals partial oxidation of the product. Typically, there are two intense peaks at 530.8 and 532.0 eV, which are assigned to *P* = O and P-O-P bonds, respectively. Although the inevitable oxidation occurred in our samples, the oxidation was reported to be beneficial for the improvement of the stability of BP (18), as was confirmed by our results as well. As shown in *SI Appendix*, Fig. S5, we can see that the positions of all of the XPS peaks and oxygen content in the 4-mo-aged BP nanosheets are almost the same as those in fresh BP nanosheets (10.5% in 4-mo-aged BP vs. 10.1% in fresh BP), indicating good stability of the BP nanosheets prepared by the bottom-up route. However, the ratio of the oxygenated species in the 4-mo-aged BP nanosheets changes notably compared with that of the fresh sample. In particular, the peak intensities at 131.8 and 132.9 eV decrease, while the peak intensity at 134.2 eV increases, suggesting the conversion of P-O-P and O-*P* = O species on the surface to P_2O_5 after 4-mo storage because of further oxidation in air. As a result, the inner BP component is protected against further oxidation. Therefore, it can be concluded that the oxidation of surface is beneficial for the improvement of stability of BP nanosheets. In addition, the optical absorption edge (*SI Appendix*, Fig. S6) and photocatalytic activity (*SI Appendix*, Fig. S7) of the samples stay almost the same as before even stored in air for 4 mo. These results further demonstrate that the BP prepared via the bottom-up route is stable, which is vital for the applications of BP as well.

Morphology and structure of the as-prepared BP were further characterized by several imaging techniques. As shown in Fig. 2*A*, a representative transmission electron microscopy (TEM) image shows a typical 2D sheet-like structure with a lateral size of 0.8–1.0 μm. Such a large size is beneficial for the application in photoelectronic devices. The scanning electron microscopy image also reveals their 2D sheet-like morphological feature (*SI Appendix*, Fig. S8). The high-resolution TEM (HRTEM) image

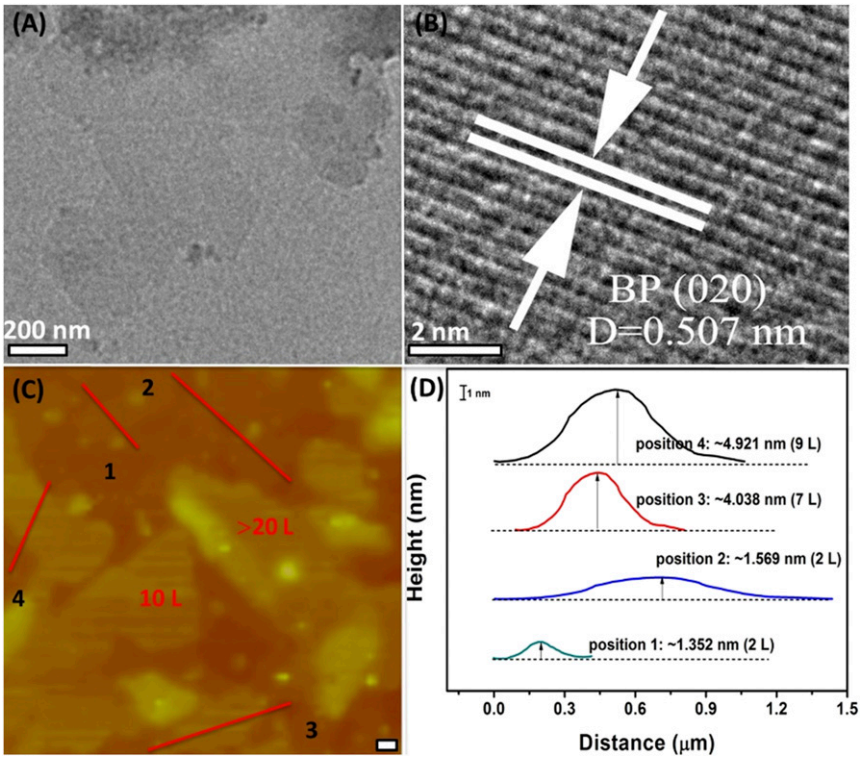

Fig. 2. TEM and AFM images of the BP nanosheets. (*A*) TEM image of the BP nanosheets. (*B*) HRTEM image corresponding to *A*. Lattice image of a BP flake shows *d* spacing of the (020) plane of orthorhombic BP. (*C*) AFM image of BP flakes. Estimated layer numbers are indicated. [Scale bar (thick white line): 0.2 μm.] (*D*) Line scans performed along the numbered lines shown in *C*. Layer numbers are identified based on their thickness. (Scale bar: 1 nm.) The BP nanosheets shown here were prepared at 100 °C.

(Fig. 2*B*) shows the lattice fringes with an interlayer spacing of 0.507 nm, corresponding to *d* spacing of the (020) plane of orthorhombic BP. The TEM images of the BP nanosheets prepared at different temperature show the flake thickness decreases with the increase of temperature until 100 °C (*SI Appendix*, Fig. S9). Further increasing temperature leads to the increase of flake thickness. Atomic force microscopy (AFM) was used to verify the sheet-like structure of the BP. As shown in Fig. 2*C*, thin BP flakes can be observed clearly in the AFM image. Multiple cross-sections were recorded of the sample laid onto a mica substrate, and a number of step heights were measured across the relief of the sample. The thickness of the BP flakes was determined to be in the range of 1–15 nm, which corresponds to 2–28 atomic layers of BP using a layer-to-layer spacing of 0.53 nm (20). This also suggests that the solvothermal method developed here is a reliable approach for the synthesis of few-layer BP nanosheets. In addition, we can also find some small-sized nanosheets in Fig. 3*C*, which have lateral size of about 100–200 nm and thickness of around 20 nm (*SI Appendix*, Fig. S10), respectively.

Our protocol for the large-scale production of few-layer BP nanosheets is conceptually simple and can be performed in all chemical laboratories. A delicate interplay is also identified between raw material and solvent. Herein, we found that ethylenediamine is a reliable medium for the formation of BP nanosheets (*SI Appendix*, Table S1). In the ethylenediamine medium, white phosphorus is not only readily solubilized, but also is transformed to a brown intermediate, which is tentatively assigned as red phosphorus based on the EDX and Raman spectra (*SI Appendix*, Fig. S11). Meanwhile, the liquid medium acts as a heat sink, which is similar to LiCl (21), further driving the reaction from the red phosphorus to BP at low temperature. Besides solvent, suitable temperature is required as well (*SI Appendix*, Table S1). There is no precipitate formed at the low temperature below 60 °C, while an unknown white crystal is obtained instead of BP over the temperature of 140 °C. The highest yield of 65% is achieved at 140 °C. Note that commercial bulk BP is very expensive [~500 US dollars per gram (USD/g)], which is the main source for the research of BP nanosheets (6, 22–24). By contrast, our synthesis cost is not more than 1 USD/g. Moreover, compared with the exfoliation technique, solvothermal method is more suitable for the large-scale synthesis of BP nanosheets.

Thermogravimetric analysis (TGA) was carried out under N_2 atmosphere to estimate the content of small molecules on the surface of BP nanosheets. We can see that the BP nanosheets have about 5% weight loss in the first weight-loss step (<350 °C) (*SI Appendix*, Fig. S12), attributed to the removal of physically adsorbed water, hydroxyl (-OH) groups and other organic species. The results also demonstrate that the content of the absorbed species on the surface of the as-prepared sample is quite low. A more dramatic weight loss starts to occur at 350 °C, associated with the decomposition of BP (20). Additionally, three exothermic peaks at 450, 500, and 520 °C are observed in the differential scanning calorimetry curve, indicating the decomposition of BP accompanied by exothermic processes (25).

BP nanosheets exhibit a thickness-dependent band gap spanning from 0.3 to 2 eV (3) for bulk and monolayer, respectively. To determine the band gap of the as-prepared BP nanosheets, therefore, the optical UV-vis–near-infrared (NIR) absorption spectra were recorded. As shown in Fig. 3*A*, a broad absorption band covering visible and NIR wavelength can be observed. Such an absorption spectrum suggests that the BP nanosheets are capable of harvesting solar energy and excellent electric conductivity. The band gap of BP nanosheets is firstly estimated to be ~1.19 eV (Fig. 3*B*) from the Tauc plot [$(ahv)^2$ vs. hv curve],

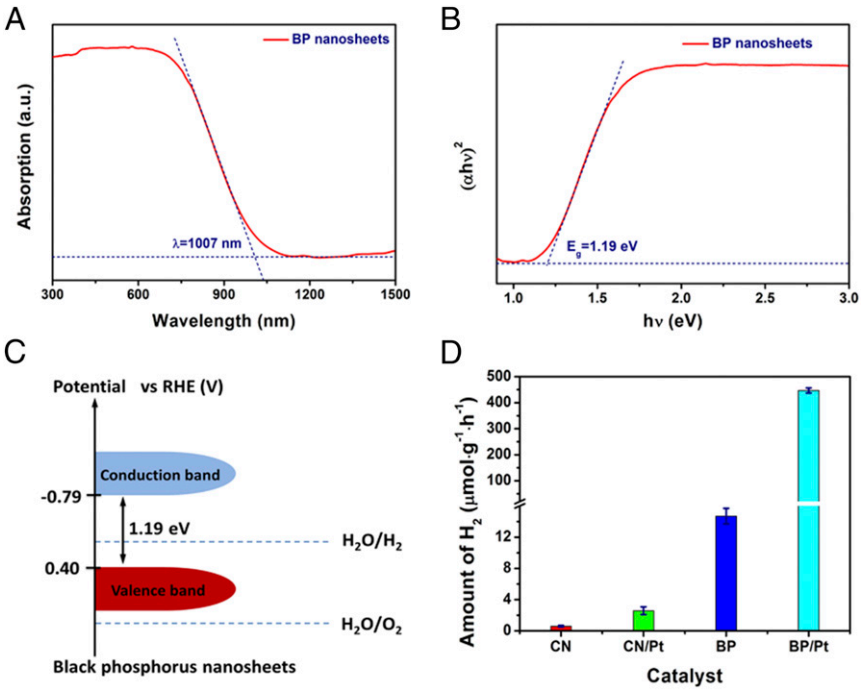

Fig. 3. Band-gap and photocatalytic hydrogen evolution of the BP nanosheets. (*A*) UV-vis-NIR absorption spectrum of the BP nanosheets. (*B*) $(\alpha h\nu)^2$ as a function of photon energy ($h\nu$), where α is the Kubelka–Munk function of the diffuse reflectance. Dashed lines show an approximate linear fit used to estimate the band edges. (*C*) Band positions of BP nanosheets according to the band-gap and flat-band potentials obtained from M-S plots and XPS valence spectra. (*D*) Hydrogen evolution rates from pure water (pH = 6.8) using BP and 20 wt % Pt/BP as catalysts under irradiation of a 300-W Xe lamp (PLS-SXE300C, $\lambda \geq 420$ nm). For a comparison, hydrogen evolution rates using C_3N_4, BP, 1 wt % Pt-enhanced C_3N_4 were measured as well.

which is consistent with the expected results from few-layer BP nanosheets (26). The few-layer BP nanosheets have been mostly focused on the application as field-effect transistors, but limited application in hydrogen evolution from water was carried out because of its stability (6, 27–29). To confirm the possibility of the as-prepared BP nanosheets as photocatalyst for water splitting, the characters of the valence and conduction bands and their absolute energies with respect to water redox potentials are analyzed by the XPS valence spectra and Mott–Schottky plots. According to the valence XPS spectra (*SI Appendix*, Fig. S13*A*), the valence-band (VB) energy level of the BP nanosheet is estimated to be ∼0.51 eV below the Fermi level. The Mott–Schottky plots (*SI Appendix*, Fig. S13*B*) shows a negative slope, suggesting the intrinsic nature of p-type semiconductor of BP nanosheets (30). The flat-band potential (E_{FB}, approximate to the Fermi level of the BP sample) is estimated to be –0.11 V [vs. reversible hydrogen electrode (RHE)] (20). Based on the band gap of BP nanosheets (1.19 eV, estimated from the UV-vis-NIR diffuse reflectance spectrum), the conduction-band and VB energy levels of BP nanosheets are calculated to be –0.79 and 0.40 V vs. RHE, respectively. Therefore, it can be envisioned that the BP nanosheets can be used as a photocatalyst for hydrogen evolution (Fig. 3*C*).

Photocatalytic hydrogen evolution experiments were performed at ambient temperature and pressure in a 180-mL Pyrex glass reactor containing 25 mg of catalyst dispersed in 110 mL of deionized water (pH = 6.8), Before irradiation using a 300-W Xe lamp coupled with a UV cutoff filter ($\lambda > 420$ nm), the reactor was thoroughly degassed by argon to remove the oxygen in the reactor. As a comparison, the photocatalytic activity of the well-known metal-free catalyst, C_3N_4 (31) was examined. As shown in Fig. 3*D*, the hydrogen evolution rate of the as-prepared BP nanosheets (14.7 $\mu mol \cdot h^{-1} \cdot g^{-1}$) is more than 24× higher than that of C_3N_4 (0.6 $\mu mol \cdot h^{-1} \cdot g^{-1}$) in pure water (31), suggesting that BP nanosheets are a promising metal-free catalyst for hydrogen evolution. Pt is an excellent cocatalyst for the improvement of photocatalytic hydrogen production rate because it can reduce the overpotential of hydrogen evolution from water (32). Indeed, the Pt-enhanced BP nanosheets exhibit an improved hydrogen evolution rate (Fig. 3*D*). The BP nanosheets prepared at 100 °C exhibit the highest hydrogen evolution (*SI Appendix*, Fig. S14). Moreover, the highest H_2 production rate can reach 447 $\mu mol \cdot h^{-1} \cdot g^{-1}$ at about 20 wt % Pt loading, which is 30-fold higher than that of bare BP nanosheets; further increasing Pt loading leads to the decrease of the H_2 production rate (*SI Appendix*, Fig. S15), ascribed to the optical shielding effect at high Pt loads (33).

More interestingly, the Pt-enhanced BP nanosheets exhibit detectable activity over the wavelength of 600 nm, which is beneficial for the utilization of solar energy. *SI Appendix*, Fig. S16 shows the apparent quantum efficiency of hydrogen evolution using 20 wt % Pt-decorated BP nanosheets. The quantum efficiencies of C_3N_4 and Pt/C_3N_4 catalysts are too low to be measured in pure water. The highest quantum efficiency is ∼4% at $\lambda = 420$ nm, which is higher than most of catalysts operated in pure water (34). Four consecutive photocatalytic reactions show no catalyst deactivation after illumination for 20 h, confirming that the Pt-decorated BP nanosheets have excellent photostability as catalyst for solar-driven hydrogen evolution (*SI Appendix*, Fig. S17). Further structural and morphological characterizations of the BP nanosheets were performed after photocatalytic reactions. As shown in *SI Appendix*, Fig. S18, we can see that there are no notable changes of the BP sample after being subjected to the photocatalytic reaction for 20 h, further confirming the stability of the BP nanosheets and its great potential for solar water splitting. The hydrogen evolution tests of BP sample after annealing at 400 °C were executed as well. As shown in *SI Appendix*, Fig. S19, we can find that the sample still maintained excellent photocatalytic stability, indicating that the trace organic molecular species has no effect on the photostability of BP nanosheets. However, the hydrogen evolution

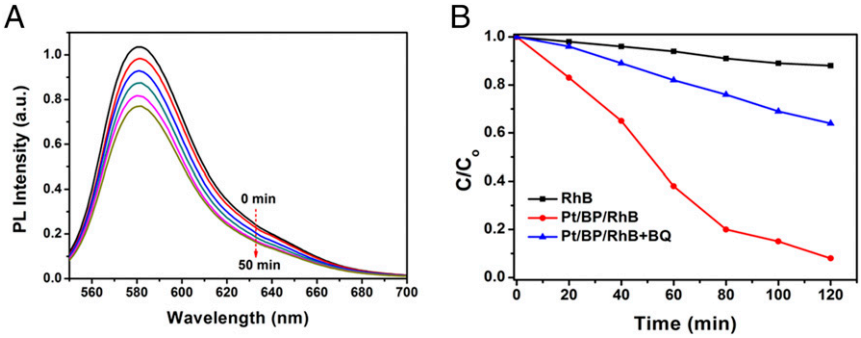

Fig. 4. Detection of oxidative product in photocatalytic reaction. (*A*) Time-dependent fluorescence emission spectra of the SFT after reaction with NO^-_2 formed from the reaction between hydroxylamine hydrochloride and $\cdot O_2^-$ over the Pt/BP catalyst under Xe lamp irradiation ($\lambda \geq 420$ nm). (*B*) Photodegradation of RhB under different conditions. Black line: pristine RhB solution; red line: RhB solution containing Pt/BP catalyst; blue line: RhB solution containing Pt/BP catalyst and 1 mmol/L benzoquinone. The light source was a 300-W Xe lamp ($\lambda \geq 420$ nm) and irradiation power was 100 mW/cm^2.

activity was decreased by 50% in comparison with the fresh BP nanosheets, which may be attributed to the decrease of active sites at high temperature (35).

Oxygen was not detected by GC, originating from high VB position of the BP nanosheets over water oxidation potential. However, the photocatalytic reactions were operated in pure water without assistance of sacrificial reagents. Therefore, it is necessary to determine the roles of photogenerated holes in the system. Some species, such as H_2O_2, $\cdot O_2^-$, or $\cdot OH$ radicals may be formed as oxydates of water by photogenerated holes. To confirm this assumption, we used hydroxylamine hydrochloride and safranine T (SFT) as fluorescent indicators for detecting $\cdot O_2^-$ radicals. The monotonic decrease of fluorescence associated with SFT is observed with the increase of irradiation time (Fig. 4*A*), confirming the existence of $\cdot O_2^-$ radicals (36). Another quencher of superoxide radicals, 1, 4-benzoquinone (BQ), was also employed to further reveal the formation of $\cdot O_2^-$ radicals under irradiation (37). As shown in Fig. 4*B*, the degradation rate of rhodamine B (RhB) decreases significantly when BQ is added to the solution, indicating that the generated $\cdot O_2^-$ radicals are captured by BQ. As a result, oxidation of RhB is suppressed greatly. These results provide a solid evidence that the photogenerated holes from the VB in the Pt-decorated BP nanosheets are powerful enough to oxidize surface-adsorbed hydroxyl groups or water to generate $\cdot O_2^-$ radicals.

On the basis of the above results, a tentative mechanism of the photocatalytic reaction is proposed (*SI Appendix*, Fig. S20). Upon the irradiation ($\lambda > 420$ nm), electron–hole pairs are generated in the BP nanosheets. The electrons diffuse to the Pt nanoparticles because of low overpotential and react with the adsorbed H^+ ions to form H_2 at its active sites. Meanwhile, the holes are mainly consumed by water or OH^- group to generate the radicals. The photocatalytic reaction along with this mechanism produces excess H^+ ions in the solution, which is consistent with the final pH value of the solution (pH is ~4).

Conclusion

In conclusion, we have developed a one-step solvothermal method for the direct preparation of BP nanosheets. It is well known that one major problem for the practical applications of BP nanosheets is their easy degradation. Given that surface coordination and covalent functionalization methods have been confirmed to work for the improvement of stability of BP nanosheets, however, these processes are complicated and time-consuming (2). By contrast, partial oxidation of surface, which is confirmed to be beneficial for the improvement of stability of BP nanosheets in this work, is more facile and feasible via this bottom-up route. The production of large quantities of partially oxidized BP nanosheets with excellent stability through a direct and facile solution-based approach will allow for the rapid development and applications of this unique 2D material. Besides promising applications in nanoelectronics (1, 12), the feasibility of hydrogen evolution using such few-layer BP nanosheets also opens up avenues for solar-driven water splitting using BP-based materials as cheap and commonly available catalyst. Interestingly, the content of oxygen in the BP nanosheets decreases after photoreaction (*SI Appendix*, Fig. S18), suggesting that the oxygen-free BP nanosheets may be obtained from the prepared partially oxidized BP nanosheets via reduction route.

Materials and Methods

Preparation of Few-Layer BP Nanosheets. Few-layer BP nanosheets were synthesized by a directly solvothermal process in ethylenediamine system using white phosphorus as raw material. In a typical synthesis process, an amount of white phosphorus was added in ethylenediamine under magnetic stirring. Subsequently, the mixture was transferred to a 100-mL Teflon-lined stainless autoclave followed by heating at 100 °C for 12 h. After cooling to room temperature naturally, the precipitates were collected and washed with benzene, ethanol, and distilled water in sequence. The final product was dried in vacuum at 60 °C overnight. Reaction temperature determines the formation and thickness of BP nanosheets. Here we confirmed the temperature in the range of 60–140 °C works for the preparation of few-layer BP nanosheets. Moreover, the higher the temperature is, the higher the yield is.

Materials Characterizations. The XRD data were obtained on a Rigaku B/Max-RB diffractometer with a Cu Kα radiation operated at 40 kV and 40 mA over a 2θ range of 10–80°. TEM and HRTEM images were recorded using a Tecnai-G2-F30 field-emission TEM with an accelerating voltage of 300 kV. High-angle annular dark-field scanning transmission electron microscopy and EDX maps were obtained on an FEI Titan operated at 200 kV. XPS was obtained by using a KRATOS Axis ultra-DLD X-ray photoelectron spectrometer with a monochromatized Mg Kα X-ray source ($h\nu$ = 1,283.3 eV). The binding energy C 1s peak from surface adventitious carbon (284.8 eV) was adopted as a reference for the binding energy measurements. AFM was performed by means of a Veeco DI Nanoscope Multi Mode V system. UV-vis-NIR diffuse reflectance spectra were obtained with a Shimadzu UV-3600 UV-vis-IR spectrophotometer. $BaSO_4$ was used as a reflectance standard. Micro-Raman spectra were obtained using a LabRam HR800 Jobin-Yvon spectrometer with an excitation wavelength of 633 nm. The TGA of BP was executed via a STA449F3 simultaneous thermal analyzer.

ACKNOWLEDGMENTS. This work was partially supported by National Natural Science Foundation of China (51302182), and The Program for the Outstanding Innovative Teams of Higher Learning Institutions of Shanxi. Work at the Molecular Foundry was supported by the Office of Science, Office of Basic Energy Sciences, of the US Department of Energy under Contract DE-AC02-05CH11231.

1. Li L, et al. (2014) Black phosphorus field-effect transistors. *Nat Nanotechnol* 9: 372–377.
2. Ryder CR, et al. (2016) Covalent functionalization and passivation of exfoliated black phosphorus via aryl diazonium chemistry. *Nat Chem* 8:597–602.
3. Kim J, et al. (2015) 2D MATERIALS. Observation of tunable band gap and anisotropic Dirac semimetal state in black phosphorus. *Science* 349:723–726.
4. Chen W, et al. (2017) Black phosphorus nanosheet-based drug delivery system for synergistic photodynamic/photothermal/chemotherapy of cancer. *Adv Mater* 29: 1603864.
5. Mannix AJ, Kiraly B, Hersam MC, Guisinger NP (2017) Synthesis and chemistry of elemental 2D materials. *Nat Rev Chem* 1:0014.
6. Favron A, et al. (2015) Photooxidation and quantum confinement effects in exfoliated black phosphorus. *Nat Mater* 14:826–832.
7. Ling X, Wang H, Huang S, Xia F, Dresselhaus MS (2015) The renaissance of black phosphorus. *Proc Natl Acad Sci USA* 112:4523–4530.
8. Reich ES (2014) Phosphorene excites materials scientists. *Nature* 506:19.
9. Wood JD, et al. (2014) Effective passivation of exfoliated black phosphorus transistors against ambient degradation. *Nano Lett* 14:6964–6970.
10. Liu H, Du Y, Deng Y, Ye PD (2015) Semiconducting black phosphorus: Synthesis, transport properties and electronic applications. *Chem Soc Rev* 44:2732–2743.
11. Sun J, et al. (2016) Entrapment of polysulfides by a black-phosphorus-modified separator for lithium-sulfur batteries. *Adv Mater* 28:9797–9803.
12. Xia F, Wang H, Jia Y (2014) Rediscovering black phosphorus as an anisotropic layered material for optoelectronics and electronics. *Nat Commun* 5:4458.
13. Bridgman PW (1914) Two new modifications of phosphorus. *J Am Chem Soc* 36: 1344–1363.
14. Rissi EN, Soignard E, McKiernan KA, Benmore CJ, Yarger JL (2012) Pressure-induced crystallization of amorphous red phosphorus. *Solid State Commun* 152:390–394.
15. Krebs H, Weitz H, Worms KH (1955) Über die Struktur und Eigenschaften der Halbmetalle. VIII. Die katalytische Darstellung des schwarzen Phosphors. *Z Anorg Allg Chem* 280:119–133.
16. Lange S, Schmidt P, Nilges T (2007) Au_3SnP_7@black phosphorus: An easy access to black phosphorus. *Inorg Chem* 46:4028–4035.
17. Lee S, et al. (2015) Anisotropic in-plane thermal conductivity of black phosphorus nanoribbons at temperatures higher than 100 K. *Nat Commun* 6:8573.
18. Zhou Q, Chen Q, Tong Y, Wang J (2016) Light-induced ambient degradation of few-layer black phosphorus: Mechanism and protection. *Angew Chem Int Ed Engl* 55: 11437–11441.
19. Zhu X, et al. (2017) Black phosphorus revisited: A missing metal-free elemental photocatalyst for visible light hydrogen evolution. *Adv Mater* 29:1605776.
20. Morita A (1986) Semiconducting black phosphorus. *Appl Phys A Solids Surf* 39: 227–242.
21. Fitzmaurice JC, Hector A, Parki IP (1994) Low-energy initiated routes to crystalline metal phosphides and arsenides. *J Mater Sci Lett* 13:1–2.
22. Kang J, et al. (2015) Solvent exfoliation of electronic-grade, two-dimensional black phosphorus. *ACS Nano* 9:3596–3604.
23. Buscema M, Groenendijk DJ, Steele GA, van der Zant HS, Castellanos-Gomez A (2014) Photovoltaic effect in few-layer black phosphorus PN junctions defined by local electrostatic gating. *Nat Commun* 5:4651.
24. Buscema M, et al. (2014) Fast and broadband photoresponse of few-layer black phosphorus field-effect transistors. *Nano Lett* 14:3347–3352.
25. Badia A, Cuccia L, Demers L, Morin F, Lennox RB (1997) Structure and dynamics in alkanethiolate monolayers self-assembled on gold nanoparticles: A DSC, FT-IR, and deuterium NMR study. *J Am Chem Soc* 119:2682–2692.
26. Qiao J, Kong X, Hu ZX, Yang F, Ji W (2014) High-mobility transport anisotropy and linear dichroism in few-layer black phosphorus. *Nat Commun* 5:4475.
27. Rahman MZ, Kwong CW, Davey K, Qiao SZ (2016) 2D phosphorene as a water splitting photocatalyst: Fundamentals to applications. *Energy Environ Sci* 9:709–728.
28. Ran J, Wang X, Zhu B, Qiao SZ (2017) Strongly interactive 0D/2D hetero-structure of a $Zn_xCd_{1-x}S$ nano-particle decorated phosphorene nano-sheet for enhanced visible-light photocatalytic H_2 production. *Chem Commun (Camb)* 53:9882–9885.
29. Ran J, Zhu B, Qiao SZ (2017) Phosphorene co-catalyst advancing highly efficient visible-light photocatalytic hydrogen production. *Angew Chem Int Ed Engl* 56: 10373–10377.
30. Liao L, et al. (2014) Efficient solar water-splitting using a nanocrystalline CoO photocatalyst. *Nat Nanotechnol* 9:69–73.
31. Wang X, et al. (2009) A metal-free polymeric photocatalyst for hydrogen production from water under visible light. *Nat Mater* 8:76–80.
32. Tian B, et al. (2017) Water splitting by CdS/Pt/WO_3-CeO_x photocatalysts with assisting of artificial blood perfluorodecalin. *J Catal* 350:189–196.
33. Yu X, et al. (2014) $Cu_{(2)}ZnSnS_{(4)}$-Pt and $Cu_{(2)}ZnSnS_{(4)}$-Au heterostructured nanoparticles for photocatalytic water splitting and pollutant degradation. *J Am Chem Soc* 136:9236–9239.
34. Fujito H, et al. (2016) Layered perovskite oxychloride Bi_4NbO_8Cl: A stable visible light responsive photocatalyst for water splitting. *J Am Chem Soc* 138:2082–2085.
35. Liu G, Niu P, Yin L, Cheng HM (2012) α-Sulfur crystals as a visible-light-active photocatalyst. *J Am Chem Soc* 134:9070–9073.
36. Elstner EF, Heupel A (1976) Inhibition of nitrite formation from hydroxylammonium-chloride: A simple assay for superoxide dismutase. *Anal Biochem* 70:616–620.
37. Ensafia AA, Kazemzadeh A (2002) Monitoring nitrite with optical sensing films. *Microchem J* 72:193–199.